Nonlinear Chirp Interference Mitigation in Snapshot GNSS Receivers Using Piecewise Least Squares Estimation With Fractional Fourier Transform

Xavier Álvarez-Molina, *Graduate Student Member, IEEE*, Gonzalo Seco-Granados, *Fellow, IEEE*, and José A. López-Salcedo, *Senior Member, IEEE*

***Abstract*—Global Navigation Satellite Systems (GNSSs) face increasing vulnerability to radio frequency interference, with chirp signals representing a particularly challenging threat due to their time-varying frequency characteristics that disrupt receivers across wide bandwidths. This study introduces a novel interference mitigation technique that partitions the interferer into segments, leveraging the fractional Fourier transform (FrFT) to enhance suppression. The proposed algorithm employs a piecewise least squares estimation method in combination with fractional-domain processing, specifically aimed at manage nonlinear wideband chirp interference impacting snapshot GNSS receivers. A generalized cross validation metric is used to balance algorithmic complexity with fitting accuracy in each segment. Mitigation occurs in the fractional domain, allowing interference energy to be concentrated at fractional coordinates matching the chirp characteristics, thereby reducing the number of affected GNSS samples compare to traditional pulse blanking. The method demonstrates particular robustness against linear frequency modulated (LFM) chirps, and for quadratic frequency modulated signals, it further divides the interference into approximately LFM segments for targeted FrFT-based suppression. Experimental results show that this approach preserves signal quality more effectively than conventional mitigation strategies.**

***Index Terms*—Antijamming techniques, fractional Fourier transform (FrFT), interference mitigation, linear frequency modulated (LFM), quadratic frequency modulated (QFM).**

I. Introduction

GLOBAL Navigation Satellite Systems (GNSSs) have become a key part of modern technology, providing positioning, navigation, and timing services in various applications. However, radio frequency interference has become a significant threat to GNSS performance and reliability. Interference types, chirp signals are particularly challenging due to the nature of their time–frequency variation, which disrupts GNSS receivers across a wide bandwidth [1], [2].

Existing chirp interference mitigation strategies span across a wide range of signal processing approaches, each offering unique advantages and limitations when implemented in GNSS receivers. The filter bank approach presented by Rügamer et al. [3] provides a method for interference suppression by decomposing the received signal into multiple time–frequency segments. This technique demonstrates effectiveness in scenarios where interference exhibits predictable patterns across discrete frequency bands and time slots, allowing for targeted filtering operations. However, the method faces inherent challenges when confronting highly dynamic interfering signals that rapidly traverse different frequency bands, potentially requiring excessive filter bank complexity. Similarly, adaptive filtering techniques, such as the adaptive notch filter (ANF) proposed in [4], introduce time-varying mechanisms that continuously update the filter parameters based on the signal statistics. This enables robust performance under varying interference conditions without requiring prior knowledge of interference characteristics. Because of their required convergence time, adaptive methods may not fit well for their implementation into snapshot GNSS receivers, where a small piece of just a few ms-long signal needs to be processed. Also, when abrupt changes on the interference characteristics are experienced. An alternative approach proposed in [5] jointly estimates GNSS parameters (time delay and Doppler shift) and mitigates constant modulus interferences by modeling interference phases with flexible von Mises priors.

Recently, fractional Fourier transform (FrFT)-based techniques [6], [7] have emerged as powerful alternatives by leveraging transformation into domains between time and frequency, where chirp linear signals can be efficiently represented and mitigated. Previous FrFT implementations in [8] and [9]

Received 31 October 2025; revised 16 March 2026; accepted 17 March 2026. Date of publication 3 April 2026; date of current version 15 April 2026. This work was supported in part by the Spanish Agency of Research (AEI) under Grant PID2023-152820OB-I00, in part by the MICIU/AEI/10.13039/501100011033, in part by ERDF/EU, in part by MICIU/AEI/10.13039/501100011033 under Grant CPP2023-010674, in part by ERDF/EU, in part by MICIU/AEI/10.13039/501100011033 under Grant PDC2023-145858-I00, and in part by the European Union NextGenerationEU/PRTR. *(Corresponding author: Xavier Álvarez-Molina.)*

The authors are with the Universitat Autónoma de Barcelona (UAB), IEEC, CERES, 08193 Bellaterra, Spain (e-mail: xavier.alvarez.molina@uab.cat).

Digital Object Identifier 10.1109/JISPIN.2026.3677784

© 2026 The Authors. This work is licensed under a Creative Commons Attribution 4.0 License. For more information, see https://creativecommons.org/licenses/by/4.0/

use exhaustive search methods in tentative fractional orders, introducing significant computational demands for a resource-constrained GNSS receivers. Other methods, such as in [10], have improved this computational complexity but with the mitigation constrained to linear chirps only.

This article addresses the limitations of current interference mitigation techniques for snapshot GNSS receivers that rely solely on the properties of the FrFT for handling linear frequency modulated (LFM) signals. The proposed method also extends to nonlinear frequency modulated (NLFM) signals, including quadratic frequency modulated (QFM) signals that have increased and varying chirp rate. The growing challenge posed by NLFM interference in modern environments requires receivers with increased robustness against this rapidly growing scenarios. Furthermore, a performance evaluation is carried out, comparing the proposed approach with established techniques, such as ANF under LFM scenarios. This comparison demonstrates the superior robustness and adaptability of the piecewise FrFT-based approach. In addition to algorithm development and empirical validation, this work thoroughly investigates the theoretical inherent limitations of the segmentation-based FrFT method. The analysis focuses on the impacts of the time–frequency resolution constraints and the sensitivity to rapidly changing chirp rates. This study makes a significant contribution to the GNSS interference mitigation field, ensuring resilient performance against increasingly complex interferences.

The rest of this article is structured as follows. Section II introduces the signal model and analyzes the types of chirps considered in this work. A brief overview of the FrFT is presented in Section III. The method for determining the fractional order to concentrate the chirp is described in Section IV, where we also present a new algorithm to represent any NLFM signal as a series of LFM segments. Section V describes the proposed excision and mitigation method, including the block-based processing strategy used for signal reconstruction, and provides a computational complexity analysis of the algorithm. Analytical limitations of the proposed method are discussed in Section VI where the constraints about time–frequency resolution are handled. To evaluate the performance of the algorithm, Section VII presents two tests: one using an LFM signal compared against existing mitigation techniques from the literature, and another using a QFM signal to demonstrate the effectiveness of the method against common NLFM types. Finally, Section VIII concludes this article with a summary of the results and main findings of this article.

II. GNSS Signal Model

Let us consider a GNSS received signal affected by an interference, leading to the following discrete-time baseband equivalent signal model:

$$x[n] = s[n] + v[n] + w[n] \tag{1}$$

where $v[n]$ represents the chirp interference signal and $w[n]$ is additive white Gaussian noise (AWGN). The GNSS signal, $s[n]$, can be ignored at this stage since it is buried below the noise floor. The chirp interference signal $v[n]$ is an FM signal, defined as

$$v[n] = A \cdot e^{j\phi[n]} \tag{2}$$

where:

1) A: Amplitude of the chirp signal;
2) $\phi[n]$: Time-varying phase encompassing the frequency variations of the chirp signal.

This article considers two types of chirp interference signals: LFM and QFM signals. Their instantaneous frequency behaviors are described as follows:

$$f_{\text{inst}}[n] = f_0 + \text{mod}_B\left(B\frac{nT_s}{T_{\text{chirp}}}\right) \tag{3}$$

$$f_{\text{inst}}[n] = f_0 + \text{mod}_B(K_1 nT_s + K_2(nT_s)^2) \tag{4}$$

where n is the sample index, $T_s = 1/f_s$ is the sampling interval, f_0 is the starting frequency, B is the chirp bandwidth, K_1 and K_2 are chirp constants specific to the QFM case, and T_{chirp} is the chirp period of the LFM. The noise term $w[n]$ is AWGN with zero mean and variance σ^2, namely

$$w[n] \sim \mathcal{N}(0, \sigma^2). \tag{5}$$

III. Fractional Fourier Transform

The FrFT is a generalization of the classical Fourier transform that provides a representation of signals in intermediate domains between time and frequency [6], [7]. It introduces a fractional order parameter, α, which determines the rotation angle in the time–frequency plane where the fractional transformation will be performed. This approach becomes interesting when dealing with LFM chirp signals, which exhibit time-varying features in both the time and frequency domains, but that become one-dimensionally time-varying when appropriately rotated in the time–frequency plane.

The continuous FrFT of a continuous-time signal $x(t)$ is defined as

$$X_\alpha(u) = \int_{-\infty}^{\infty} x(t)K_\alpha(t,u)dt \tag{6}$$

where the kernel $K_\alpha(t,u)$ is given by

$$K_\alpha(t,u) = \begin{cases} A_\alpha e^{j\pi(t^2 c_\alpha - 2tuc_\alpha^{-1} + u^2 c_\alpha)}, & \alpha \neq k\pi \\ \delta(t-u), & \alpha = 2k\pi \\ \delta(t+u), & \alpha = (2k+1)\pi \end{cases} \tag{7}$$

with $A_\alpha = \sqrt{1 - jc_\alpha}$, $c_\alpha = \cot(\alpha)$, and k being an integer.

For discrete-time signals, the FrFT is computed using discrete algorithms that efficiently approximate its continuous-time counterpart. The discrete fractional Fourier transform (DFrFT) preserves key properties of the continuous FrFT while operating on sampled data. The DFrFT used in this article is the one defined in [6] and implemented in [7]. It is expressed as

$$X_\alpha[k] = \sum_{n=0}^{N-1} x[n]K_\alpha[n,k] \tag{8}$$

where $K_\alpha[n,k]$ is a discretized version of the kernel. The FrFT is particularly suited for chirp signal analysis due to its ability to represent signals in rotated time–frequency domains. By selecting an appropriate fractional order α, chirp signals can be transformed into a compact representation in the fractional

domain, enabling effective interference mitigation in GNSS systems. The relationship between the chirp rate of the interfering signal and α that maximizes the concentration of energy in a few bins of the DFrFT is defined by the kernel function with the following equation:

$$\hat{\alpha} = \frac{2\cot^{-1}(\hat{k}_{\text{chirp}} D)}{\pi} \tag{9}$$

where $\cot^{-1}$ is the inverse cotangent, $\hat{k}_{\text{chirp}}$ is the estimated chirp rate of the interfering signal, and D is a normalization factor defined by $\frac{N}{f_s^2}$ that can be derived by the resolution of the DFrFT used.

IV. Fractional Order Identification

Previous methods for searching the optimal fractional order α typically rely on exhaustive and computationally intensive search procedures. For instance, the approaches presented in [8], [9], and [11] use the FrFT to mitigate interference by iterating across all possible α values and selecting the one that maximizes the concentration of signal energy in the fractional domain. Our proposal is to reduce the computational complexity of this intensive search procedures by obtaining an estimation of α based on time–frequency plane analysis.

The proposed method begins by estimating the instantaneous frequency behavior of the interfered signal. This is achieved by computing the short time Fourier transform (STFT) and extracting the frequency trajectory through a time–frequency ridge (TFR) algorithm, resulting in a vector that represents the instantaneous frequency evolution over time. Next, the algorithm analyzes this frequency vector to detect the signal's periodicity. Once the periods are identified, each period is independently segmented using a piecewise least squares estimation (PLSE) approach.

This segmentation divides the period into multiple approximately linear fragments, allowing the local chirp rate of each segment to be accurately estimated. This segmentation enables precise estimation of the chirp rate for each fragment. The PLSE approach facilitates computing the slope for each segment, which corresponds directly to the chirp rate. At each segment, the chirp rate may vary depending on the frequency of the signal, allowing the maximum concentration of energy on the fractional domain.

A. TFR Extraction Algorithm

The TFR algorithm is able to identify and extract the most prominent energy ridges in the time–frequency representation of a signal. In our case, these are the ridges contained in the STFT, which correspond to the instantaneous frequency components of the chirp interference. The procedure for extracting such ridges follows a forward–backward greedy optimization approach [12], [13]. The algorithm operates using the following inputs.

1) $\mathbf{T}$: Time–frequency matrix of size $M \times N$, where M is the number of frequency bins and N is the number of time samples.
2) $\mathbf{f}$: Frequency vector containing the frequencies of each row of matrix $\mathbf{T}$.

Algorithm 1: Piecewise Linear Least Squares with GCV.

Require: Signal y, parameters $n_{\min}$, $n_{\max}$
Ensure: Optimal segmentation and fit
if y is discontinue **then**
  Divide y into continue segments
end if
for $n = n_{\min}$ **to** $n_{\max}$ **do**
  Divide y into n segments (as equal as possible)
  for each segment **do**
    Fit a line (least squares) to the segment
  end for
  Compute total MSE for all segments
  Compute GCV score:

$$\text{GCV}(n) = \frac{\bar{\text{MSE}}(n)}{(1 - \frac{2n}{N})^2}$$

end for
Select n^* that minimizes GCV(n)
Output segmentation and fit for n^*

3) $P \geq 0$: Penalty parameter that discourages large frequency jumps between adjacent time steps.

In a simplified manner, for each time step $j = 1, 2, \ldots, N$, the algorithm identifies the frequency bin i that maximizes the energy function

$$E_{i,j} = T(i,j) - P \cdot |f_i - f_{i-1}|^2 \tag{10}$$

where $T(i,j)$ is the energy at frequency bin i and time sample j, f_i is the actual frequency, and f_{i-1} is the previous frequency. The ridge frequency at time step j is given by [13]

$$i_j = \underset{i \in \{1,\ldots,M\}}{\arg\max} \left\{ T(i,j) - P \cdot |i - i_{j-1}|^2 \right\} \tag{11}$$

where a maximization of the frequency bin i at every time period j is done, thus providing the sets of frequencies where the energy is located and extracted as

$$f_{\text{ridge}}(j) = \mathbf{f}(i_j) \quad \forall j \in \{1, \ldots, N\}. \tag{12}$$

Note that in our environment, the algorithm is reduced to only estimating the main ridge on the time–frequency matrix and not to manage other ridges. A detailed description of the algorithm can be found in [14].

B. Generalized Chirp Rate Estimation Method

The fundamental concept of this method lies on dividing the extracted instantaneous frequency ridges into various segments. Each of these segments can be approximated by a linear frequency shift, facilitating the subsequent application of the FrFT and its subsequent interference mitigation. Following this step, Algorithm 1 can be executed to perform the estimation of the chirp rate and the definition of the segmented linear components. Subsequently, this approach enables the use of the FrFT to mitigate affected samples at each segment.

The first step of the algorithm is to divide the signal into the different periods. The detection of these periods is done

by computing the differences between each bin of frequencies extracted; if these differences exceed a given threshold of frequency, then the signal will be considered to be discontinued. After that, the idea behind the algorithm is dividing each period of signal into equal segments and computing the mean-squared error (MSE) between the obtained frequency vector and the linear fitting obtained with PLSE for all the segments. Using the least squares estimator (LSE) inside each segment allows the algorithm to obtain an estimation of the slope (chirp rate) and intercept (initial frequency) of the frequency ridges of the signal. LSE fits a linear model by minimizing the sum of squared residuals between observed data and model predictions. Given measurements $\mathbf{y}$ and model matrix $\mathbf{A}$, LSE finds

$$\hat{\boldsymbol{\theta}} = (\mathbf{A}^T\mathbf{A})^{-1}\mathbf{A}^T\mathbf{y} \tag{13}$$

where $\hat{\boldsymbol{\theta}}$ is a matrix containing both intercept and slope, $\mathbf{A}$ is the design matrix, and $\mathbf{y}$ is the frequency data. Under the condition that $\mathbf{A}^T\mathbf{A}$ is full rank. If we employ only the MSE as a metric, then the algorithm will tend to overfitting, by segmenting into a number of segments close to the maximum possible.

To minimize the overfitting effect and not reach the maximum segment number, a cost function was designed with the aim of reducing the number of required segments. The generalized cross-validation (GCV) metric [15], [16] employs the mean square error or alternative metrics representing the discrepancy between the fitted and actual data, adding a term to assess system complexity. In our analysis, the degrees of freedom for the fitting are set at two due to the linear estimation of the slope and intercept. Consequently, the factor directly influencing complexity is the product of the number of segments and the degrees of freedom, divided by the total number of data points utilized. As the segment count rises, the GCV metric notably decreases. This results in selecting the most suitable and least complex fitting solution. The metric is as follows [15], [16]:

$$\mathrm{GCV}(n) = \frac{\bar{\mathrm{MSE}}(n)}{(1-\frac{2n}{N})^2} \tag{14}$$

where $\bar{\mathrm{MSE}}(n)$ is the mean of MSE of each segment, n is the number of segments tried, and N is the total number of data used in the segment. To show the derivation of the metric, the general base formula for the GCV metric is defined as

$$V = \frac{\left\|(\mathbf{I}-\tilde{\mathbf{H}})\tilde{\mathbf{y}}\right\|^2/N}{\left(1-\frac{1}{N}\,\mathrm{tr}(\tilde{\mathbf{H}})\right)^2} \tag{15}$$

where the numerator clearly represents the MSE comparing the fitted results $\tilde{\mathbf{H}}\tilde{\mathbf{y}}$ with the data $\tilde{\mathbf{y}}$ itself. The denominator contains a term controlling the complexity through the design matrix, which can be expressed as

$$\tilde{\mathbf{H}} = \tilde{\mathbf{X}}(\tilde{\mathbf{X}}^*\tilde{\mathbf{X}})^{-1}\tilde{\mathbf{X}}^* \tag{16}$$

where $\tilde{\mathbf{X}}$ is the design matrix of the segment, whose first column accounts for the intercept and whose second column contains the sample indices $k = 0, \ldots, L_s - 1$. Using the properties of the trace operator, particularly its cyclic property and the identity that the trace of an identity matrix equals its dimension, we obtain that $\mathrm{tr}(\tilde{\mathbf{H}}) = 2n$ that represents 2 degrees of freedom on each segment used for the model, which penalizes the increase in number of segments, balancing fitting accuracy and model complexity to avoid overfitting. In Fig. 2, an example of the segmentation of QFM and LFM signals is shown. Note how in places where the chirp is more curved, the algorithm uses more segments to define it, as compared to where the chirp exhibits a more linear behavior. The corresponding GCV score is shown in logarithmic scale at Fig. 3 to check the behavior of the algorithm versus different number of segments. For the linear one, the use of more segments does not reduce the MSE enough to compensate the increase of complexity. For the case of the QFM, the algorithm is allowed to add segments that reduce the ratio of MSE and complexity up to a given point where the ratio is stabilizes and more segments are not useful. On each of the segments obtained from this algorithm, the mitigation found in Section V will be applied.

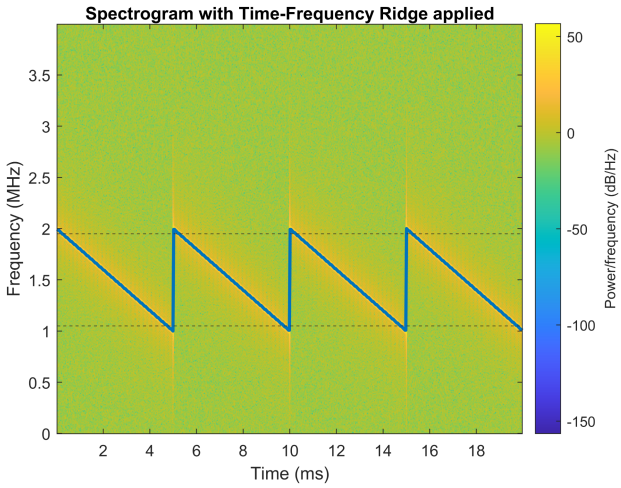

Fig. 1. Spectrogram of the linear chirp signal with the TFR method superposed. $T_{\text{chirp}} = 5$ ms, $BW = 1$ MHz, $f_0 = 1575.42$ MHz, and JNR $= 40$ dB.

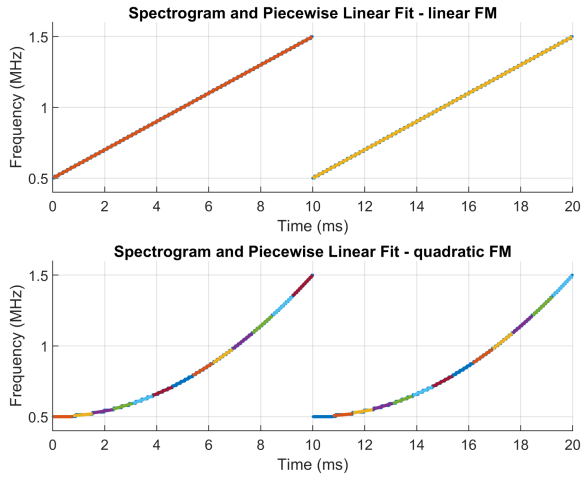

Fig. 2. Frequency behavior of LFM and QFM signals. The frequency is directly shown as base and the colored lines represent the segmentation obtained from Algorithm 1.

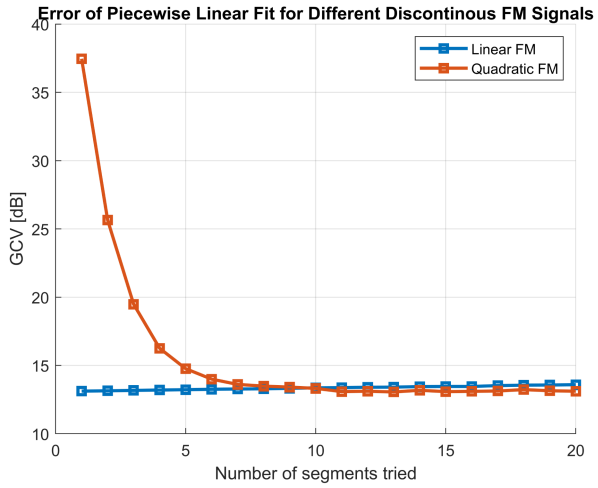

Fig. 3. GCV score evolution for both LFM and QFM signals in Fig. 1 along the segments tried.

V. Fractional-Domain Mitigation Technique

The mitigation of the interference is performed in the fractional domain once the NLFM signal has been approximated as a sequence of linear-frequency segments. This section describes the proposed fractional-domain interference mitigation procedure and the block-based implementation used for signal reconstruction. In addition, the computational complexity of the overall algorithmic pipeline is analyzed.

A. Fractional-Domain Interference Mitigation

Once the NLFM interference signal is divided into approximately linear-frequency segments, we can now apply the filtering on the fractional domain using the segmentation obtained from Algorithm 1. We already computed the chirp rate of each segment, thanks to the LSE applied. The use of the fractional domain allows a concentration of the chirp component. This concentration effect occurs because the FrFT effectively aligns the transformed domain with the chirp's time–frequency structure, resulting in a compact representation that resembles an impulse or narrowband signal rather than a wideband one. This property creates an ideal scenario for applying excision techniques, which can effectively remove the interference while preserving most of the desired GNSS signal content. The property of the sum of indexes of the FrFT can be used to recover the signal, and doing the transformation with an α order can be reversed by doing the transformation of $-\alpha$ order.

A practical challenge arises during reconstruction when processing is performed blockwise: discontinuities or transient artifacts may occur at block boundaries, generating spurious effects in the final combined signal. These effects are not solely caused by blockwise filtering, but also by the segmentation of the signal itself. In addition, the filtering is done by different time-varying finite impulse response filters depending on the location of the interference segment, and also on different fractional domains with different α. For that reason, it is a key to mitigate these artifacts and maintain signal integrity. To do so, the overlap-and-save method is employed. This strategy ensures smooth transitions between blocks, suppressing boundary artifacts and avoiding

Algorithm 2: Overlap–Save Method for Fractional Domain and Time Varying Filtering.

Require: Input signal $x[n]$, Segmentation of the Input signal into equal segments of N samples, $\hat{\alpha}$ of each segment.
Ensure: Output signal $y[n]$ (filtered signal without interference)
Initialize position index $pos \leftarrow 0$
while $pos + N \leq \text{length}(x)$ **do**
  Extract segments: $x_{\text{block}} \leftarrow x[pos : pos + N - 1]$
  if pos $= 0$ **then**
    Prepend $M - 1$ zeros to the first block if needed
  else
    Prepend the tail from previous block
  end if
  Apply Hann window to the block to be processed: W_{Hann}
  Compute FrFT of input block: $X_{FrFT} = \text{FrFT}(x_{\text{block}} \cdot W_{Hann}, \hat{\alpha})$
  Apply PB in the fractional domain: $Y_{FrFT} = X_{FrFT} \cdot M$, where M is the mask of the complex signum filter.
  Compute inverse FrFT: $y_{\text{block}} = \text{FrFT}(Y, -\hat{\alpha})$
  Save first $M - 1$ samples of y_{block} (corrupted samples due to circular convolution)
  Append remaining samples to output $y[n]$
  Increment index: $pos \leftarrow pos + (N - M + 1)$
end while

the introduction of spurious components between processed segments that can be harassing due to the conditions of the filtering. Applying a Hann or Hanning [17] window can smooth even better the edges of each block, reducing discontinuities between the mitigation process. This method is described in Algorithm 2 shown next.

Algorithm 2 starts with the segmentation of the input signal into different fragments, which are obtained from Algorithm 1, and $\hat{\alpha}$ obtained for each fragment. Then, it starts iterating over the segments, preappending zeros based on the overlap previously defined. After windowing the segment, we apply the FrFT to obtain a concentrated version of the interference in the segment, we apply the pulse blanking method, and return to the time domain by applying the inverse transformation, we discard the preappended samples to the segment and at last, we add this segment to the output signal, with no interference component.

As shown previously, the mitigation process follows a structured approach beginning with the use of the segmented signal in order to perform a block processing. To achieve this mitigation on each block, we adopt the complex signum nonlinearity method [18]. The idea is to mitigate only the signal components on the fractional domain that are affected by interference. For signals transformed into the fractional domain, the processing operation becomes

$$X_{\alpha,\text{CS}}[k] = \begin{cases} \frac{X_\alpha[k]}{|X_\alpha[k]|}, & \text{if } |X_\alpha[k]| > \gamma \\ X_\alpha[k], & \text{otherwise} \end{cases} \tag{17}$$

where $X_\alpha[k]$ represents the kth component of the signal in the fractional domain with rotation angle α, $|\cdot|$ denotes the absolute value, and γ denotes the decision threshold. This operation effectively preserves the phase information while normalizing the amplitude.

The threshold γ was derived using a Weibull distribution fitted to empirical data collected under interference-free conditions (GNSS signal + background noise). The Weibull model effectively captured the amplitude statistics in the fractional domain, enabling computation of γ for a false alarm probability $P_{\text{FA}} = 10^{-7}$. This threshold serves as a decision boundary, enabling the detection algorithm to reliably distinguish between the chirp component and the GPS signal component on the fractional domain.

B. Complexity Analysis

The computational complexity of the proposed algorithm can be decomposed into its four constituent elements: STFT computation, TFR extraction, PLSE segmentation, and fractional-domain mitigation.

Regarding the first element, the STFT processes a total of N input samples divided into segments of M samples each. The number of segments to process therefore becomes $K_s = N/M$. Since each segment involves computing an M-points fast Fourier transform (FFT), whose complexity is known to be $O(M \log M)$, the resulting complexity of the STFT stage becomes $O(K_s M \log M) = O(N \log M)$.

Next, the ridge extraction stage searches the maximum among the M FFT frequency bins on each of the K_s STFT segments. Since the complexity of searching the maximum value in M elements is $O(M)$, the resulting complexity becomes $O(K_s M) = O(N)$.

The PLSE segmentation stage operates on the instantaneous frequency ridge obtained from the STFT. Since each STFT segment leads to one ridge sample, the resulting ridge vector contains a total of K_s samples. The latter are then divided into K_p disjoint subsegments of K_s/K_p samples, each containing one chirp period. Each subsegment is further divided into K_{LS} intervals of $\frac{K_s}{K_p K_{\text{LS}}}$ samples each, where LS estimation is implemented for determining the slope (i.e., chirp rate) and intercept of the values contained within each interval. Since the complexity of such LS estimation scales as twice the number of samples [19], the complexity for each LS interval becomes $O(2\frac{K_s}{K_p K_{\text{LS}}})$ and the total complexity over the $K_p K_{\text{LS}}$ intervals results in $O(2K_s) = O(2N/M)$.

Finally, the fractional-domain mitigation technique is implemented on each of the aforementioned $K_p K_{\text{LS}}$ intervals of $\frac{K_s}{K_p K_{\text{LS}}}$ samples each, where the linear LS estimation is carried out for determining the chirp rate. The latter is then converted into the fractional order to be used for the FrFT. Since the FrFT computation is usually implemented using the FFT, and only one fractional order is needed, the complexity of this individual FFT-based is $O(\frac{K_s}{K_p K_{\text{LS}}} \log \frac{K_s}{K_p K_{\text{LS}}})$ and the total complexity becomes $O(K_s \log \frac{K_s}{K_p K_{\text{LS}}}) = O(\frac{N}{M} \log \frac{N}{M K_p K_{\text{LS}}})$.

Adding all these four computational complexities together, it is found out that the first term is the dominant one, leading the overall asymptotic complexity of the proposed technique driven by $O(N \log M)$. In contrast, the ANF considered later in Section VII as a reference benchmark technique is known to have a lower computational complexity of $O(N)$, which explains its widespread adoption in many practical interference mitigation problems. Nevertheless, the results in Section VII will confirm the effectiveness of the proposed technique and the performance gains it provides.

VI. Analytical Limitations

Several theoretical constraints must be considered on this method, one of them being the Nyquist theorem. We need to be able of representing the FM signal on the time–frequency domain, and therefore

$$f_s \geq 2B. \tag{18}$$

Under this condition, the minimum sampling frequency to use will be directly related with the bandwidth of the chirp signal. On the other hand, we have a limitation in terms of samples to define the linear behavior of the chirp. This problem is related to the fact that chirp rate estimation is obtained from a line-fitting problem using a limited number of samples. These samples come from a spectrogram computed using the STFT, which is based on STFT that segments the input signal. The relationship between the and the spectrogram is as follows:

$$\begin{cases} N_{s,w} = \frac{T_{\text{chirp}}}{T_w} \\ T_{\text{w}} = \frac{N_w - N_o}{f_{\text{s}}} \end{cases} \tag{19}$$

where $N_{s,w}$ is the number of samples of each STFT time window, T_w is the time duration of each STFT window, N_w is the number of samples per STFT window, and N_o is the number of overlapped samples. Establishing these relationships, we can now deduce the constraint to be fulfilled

$$T_{\text{chirp}}^{\min} = \frac{N_w^{\min}(N_w - N_o)}{f_s}, \quad \text{if } N_{\min W} > 3 \tag{20}$$

where $N_{\min W}$ is the number of minimum windows inside a period. It is well known that while the LSE requires a minimum of two samples to solve a line-fitting problem, practical considerations for reliable chirp rate estimation require much more samples to achieve adequate precision.

To evaluate this fundamental limit, a simulation is conducted to analyze the relationship between temporal resolution and estimation accuracy under varying overlap processing conditions. A fixed sampling frequency of 4 MHz, and chirps starting at 15 up to 1 μs of period are evaluated. Each synthetic chirp has fixed bandwidth of 1 MHz and an SNR of 40 dB. The test is done performing an STFT with Hann window of $N_{s,w} = 16$ samples, 512 FFT points, and varying overlap samples N_o from 8 to 14. Then, using the algorithm in Section IV-A, the frequency ridges are extracted, and at last, an LSE is applied in order to compute the chirp rate.

The results of this computation are found in Fig. 4, where the performance metric is the relative estimation error between the known true chirp rate and the one estimated by the LSE method.

When only a single time sample and one frequency measurement are available, the system reduces to a 1×2 design

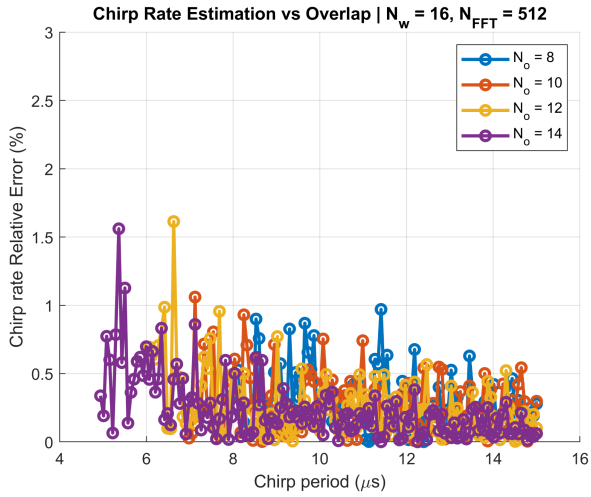

Fig. 4. Fixed chirp bandwidth with sweep of chirp period tested under different STFT configurations.

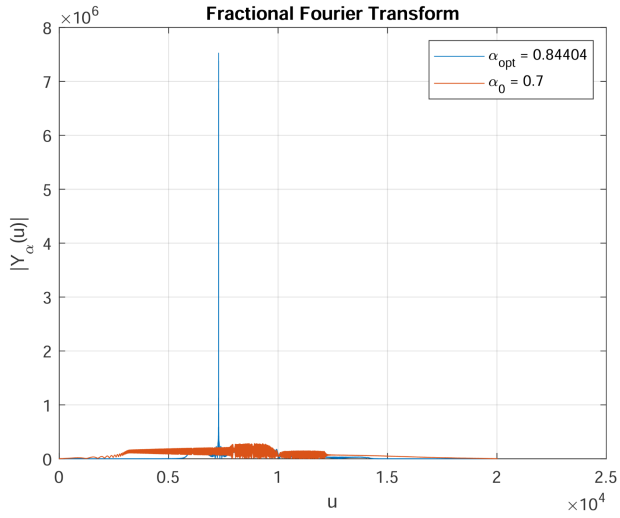

Fig. 5. DFrFT using different alpha, one with the optimal alpha, and another with erroneous one.

matrix, making $\mathbf{A}^T\mathbf{A}$ singular; the LSE solution cannot estimate slope or intercept. With exactly two time samples and two matching frequency measurements, the 2×2 system becomes invertible, but it still yields only slope and intercept estimates from one interval, resulting in extreme sensitivity to noise. In practice, estimating both slope and intercept reliably demands at least three time–frequency pairs (3×2 design but 2×2 normal matrix) to ensure full-rank conditions and reduce variance.

In our experiment, chirps with fewer than three STFT windows inside a chirp period failed to produce meaningful estimates, and those with fewer than ten pairs exhibited high error. By increasing overlap and thus time resolution, more frequency points become available within each chirp period, shifting the system away from its underdetermined and noise-sensitive limits. In practice, the minimum chirp period reliably computable was 5 μs, for which at least ten windows per segment are required to attain a reasonable chirp-rate estimation. For the effects on the mitigation process, any error on the chirp rate estimation can sharply affect the computation of the optimal alpha, causing the chirp not being concentrated as expected on the fractional domain. In Fig. 5, the impact of using a nonoptimal fractional order α in the fractional Fourier domain is illustrated. When α deviates from its optimal value, the chirp signal becomes dispersed across a broader fractional bandwidth. This dispersion causes the mitigation process to affect a larger portion of the GNSS signal samples, reducing the effectiveness of interference suppression as the signal energy is less concentrated. Consequently, the filter struggles to isolate and mitigate the interference precisely, leading to diminished performance.

VII. Performance Analysis

In this section, two different analyses are done, one using LFM signals, which are compared with different configurations of the ANF, and then, a test using QFM signals that will demonstrate the capability of the method to adapt versus different kind of frequency modulations of the signals.

A. Experimental Setup

The experimental setup consists of a Skydel GSG-8 GNSS simulator that is used to generate realistic IQ samples containing the GNSS signals of the scenarios under test. These IQ samples are then processed using the UAB snapshot GNSS software receiver, an in-house development that is able to compute the user's position and time by processing GNSS signals using an open-loop or so-called *acquisition-only* approach. The latter is efficiently implemented by means of the double FFT algorithm originally proposed in [20]. More details about this algorithm can be found in [21], and about the overall software receiver in [22, Sect. 3.8].

The GNSS scenario generated with the Skydel GSG-8 simulator corresponds to a receiver located at 41.495° longitude, 2.119° latitude, and 200 m height, with a start time on 24 June 2021 at 12:00:00 UTC. Under these conditions, eight GPS satellites are visible. The antenna model used in the simulator corresponds to the default standard antenna provided by Skydel, without any additional modifications. The simulator generates GPS L1 C/A signals at 12.5 MHz sampling rate with 16-bit quantization, which are subsequently resampled to 4 MHz. After resampling, the interference signal is synthetically generated in software and added to the IQ samples of the GNSS signals, emulating the fact that the interference went through the analog-to-digital converter (ADC) of a real GNSS hardware front end without distortion, preserving the original 16-bit dynamic range. The jammer-to-noise Ratio (J/N_0) is set to 40 dB.

The snapshot receiver is then configured to process snapshots of 20 ms length. A total of 1200 snapshots are processed per scenario, where the first 200 snapshots are interference-free in order to make sure that the receiver is first operating correctly, and then, once the interference appears, troubles are experienced and mitigation is needed.

B. LFM Signals

This test was conducted employing LFM signals with a bandwidth fixed at 1 MHz and a linear reduction of the chirp

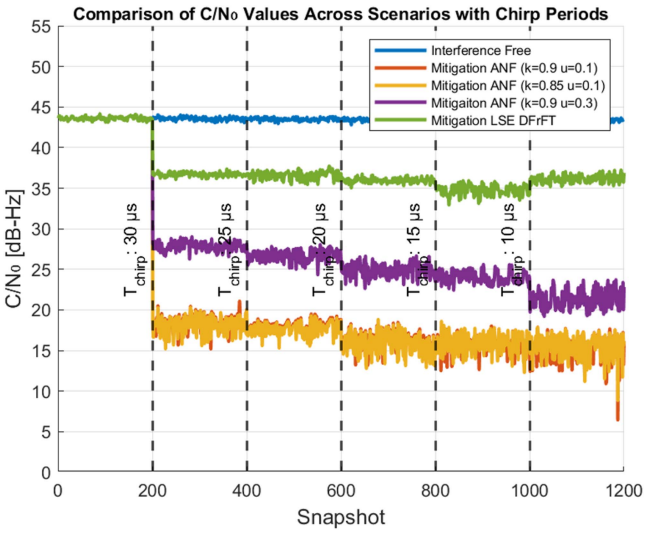

Fig. 6. C/N_0 acquired satellites DFrFT, interference free, ANF with different configurations.

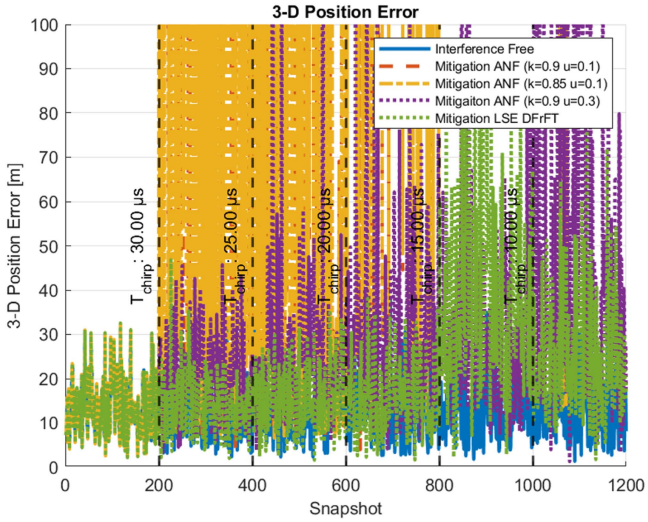

Fig. 7. 3-D position error DFrFT, interference free, ANF with different configurations.

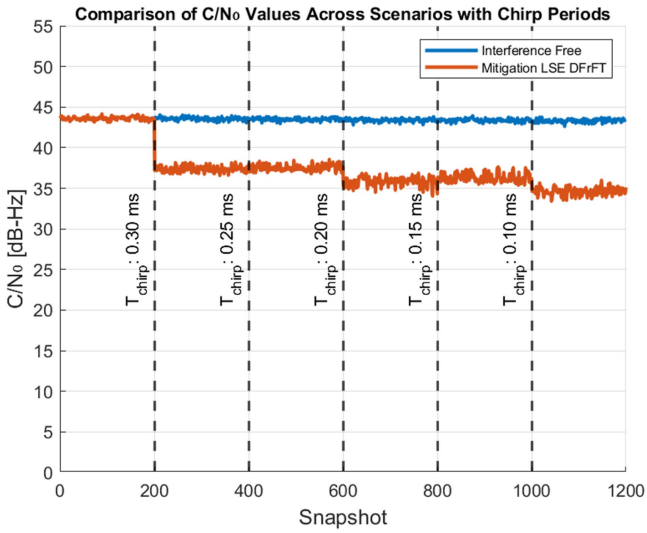

Fig. 8. C/N_0 acquired satellites in interference free and LSE FrFT method with QFM interference.

period by 5 μs every 200 snapshots starting at 30 μs. For the FrFT-based method, the configuration entailed reducing the number of samples per window in the STFT in order to reach the minimum chirp period mitigable by the method, thereby enabling finer time resolution within each chirp period at the expense of reduced frequency resolution. This adjustment clearly enhanced the method's capability to estimate the chirp rate for faster chirp signals compared to previous approaches reported in [10]. To compare with, three different ANF configurations were evaluated: two with a slow learning rate $(u = 0.1)$ but different notch widths $(k = 0.85, 0.9)$, and one with faster learning rate $(u = 0.3)$ while maintaining a fixed notch width. Results indicate that FrFT technique outperforms all tested ANF configurations in terms of C/N_0 preservation. Position domain analysis demonstrates that the ANF configuration with $k = 0.85, 0.9$ and $u = 0.1$ struggled to adequately track the frequency variations of the LFM interference.

The $k = 0.9$ and $u = 0.3$ ANF performed satisfactorily for slower chirps by effectively suppressing the interference without affecting the GPS signal; however, as chirp rates increase, the filter's performance degrades due to instability and insufficient adaption speed. Conversely, the FrFT approach consistently mitigated the interference in the fractional domain, achieving better performance both in C/N_0 and positioning error metrics. Nevertheless, for the extreme case where the chirp period reaches 20 μs, performance deteriorates owing to an insufficient number of STFT windows within the chirp intervals, which increases chirp rate estimation error and reduces the concentration efficiency of the mitigation process. The results in terms of C/N_0 can be found in Fig. 6 and the results in terms of position error in Fig. 7. As seen with the C/N_0 results, the lack of precise mitigation on the methods causes the position error to be less robust and more unstable. For the nonoptimally configured ANF, the effects are clear, and no position fix or high error values are found; for the FrFT method, the results still being robust under 100 m of position error. This demonstrates that the method not only is adapted to NLFM interferences but still working as expected in LFM scenarios.

C. QFM Signals

In this test, a QFM is superimposed to the scenario. The QFM signal is also confined in 1 MHz of bandwidth starting also at GPS L1 C/A central frequency. Note that, the chirp period in this case is reduced 0.05 ms starting at 0.30 ms every 200 snapshots. Then, the complete signal with the base nominal scenario plus the interference is processed and mitigated only using the LSE FrFT method. The objective is to shown that our PLSE FrFT method is able to mitigate not only LFM but QFM like signals.

In Fig. 8, the results in terms of C/N_0 are shown. The method demonstrates a strong capability to recover the majority of the power of the initial GPS L1 C/A signal in terms of C/N_0. An observed loss of approximately 6 dB occurs when the interference

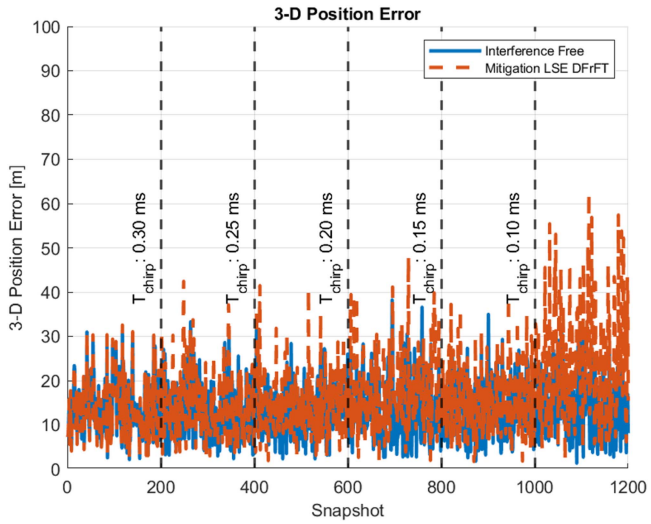

Fig. 9. 3-D position error interference free and LSE DFrFT method with QFM interference.

first enters the system, which is then sustained during the initials chirp periods of 0.30 and 0.25 ms. However, at the reduction of the 0.20 ms chirp period, a sharp decrease in the number of STFT windows occurs, even though, the algorithm still being able to estimate the chirp rate and concentrate the energy of the chirp in few frequency bins for each segment. The faster the chirp, the more the loss incurred.

Once the results in terms of C/N_0 are analyzed, the results in terms of position fixing are shown in Fig. 9. The system successfully computes the position throughout all the simulation maintaining errors within acceptable bounds. It is only during the final stages, when the chirp periods reduce to 0.1 ms, that the position error begins to exceed 40 m. This increase error is indicative of the growing difficulty in effectively mitigating the interference as the chirp rates vary from the linear ones and the chirp rate intensifies. Despite this degradation both in C/N_0 and position error, the mitigation method shows resilience by providing position estimates rather than complete signal loss or failure on position fixing. Successfully achieving robust adaption for NLFM signals, particularly demonstrating strong performance with QFM signals, represents a significant advancement in interference mitigation.

VIII. Conclusion

This work applied the FrFT-based mitigation framework to the complex and challenging domain of nonlinear wideband chirp interference affecting snapshot GNSS receivers. An algorithm is proposed for segmenting the interfering signal using piecewise LSE, and then mitigating each segment in its fractional domain. To do so, the appropriate fractional rotation α is found that concentrates most of the chirp interference signal in the smallest transformed support.

Results using realistic signals from a Skydel simulator demonstrated the robustness of the proposed approach against both standard LFM and rapidly varying QFM interference sources. Such results revealed that the FrFT approach provided superior C/N_0 preservation as compared to traditional interference mitigation methods. The method was also extended to NLFM signals, such as QFM. To do so, a piecewise LSE combined with a GCV metric was used to optimally divide a QFM chirp into LFM segments.

Nonetheless, some practical challenges remain, especially under general nonlinear chirp scenarios. When the interfering signal requires more granular segmentation, such as with QFM, the reduction in samples per segment limits the ability of the method to reach faster chirps due to the loss of samples per segment. This often leads to partial loss of signal integrity due to the mitigation process and, consequently, degraded positioning performance and C/N_0 values when compared to LFM cases. These findings highlight a key limitation: the tradeoff between segment length for local fit reliability and the ability to mitigate only interference components due to the lower number of samples of the transformation.

Future work will focus on improving the capability of the proposed method to mitigate faster interference signals by exploring new techniques that increase the time resolution of the time–frequency analysis, and comparing the results with a wider set of existing interference mitigation techniques.

References

[1] D. Borio, C. O'Driscoll, and J. Fortuny, "GNSS jammers: Effects and countermeasures," in *Proc. ESA Workshop Satell. Navigation Technol.*, Noordwijk, The Netherlands, 2012, pp. 1–7.

[2] R. H. Mitch et al., "Signal characteristics of civil GPS jammers," in *Proc. Int. Tech. Meeting Satell. Division Inst. Navigation*, 2011, pp. 1907–1919.

[3] A. Rügamer et al., "Chirp mitigation for wideband GNSS signals with filter bank pulse blanking," in *Proc. Int. Tech. Meeting Satell. Division Inst. Navigation*, 2017, pp. 3924–3940.

[4] D. Borio, L. Camoriano, and P. Mulassano, "Analysis of the one-pole notch filter for interference mitigation: Wiener solution and loss estimations," in *Proc. Int. Tech. Meeting Satell. Division Inst. Navigation*, 2006, pp. 1849–1860.

[5] J. Lesouple and L. Ortega, "Bayesian EM approach for GNSS parameters of interest estimation under constant modulus interference," *EURASIP J. Adv. Signal Process.*, vol. 2024, 2024, Art. no. 32.

[6] H. Ozaktas, O. Arikan, M. Kutay, and G. Bozdagt, "Digital computation of the fractional Fourier transform," *IEEE Trans. Signal Process.*, vol. 44, no. 9, pp. 2141–2150, Sep. 1996.

[7] A. Bultheel and H. E. Martínez Sulbaran, "Computation of the fractional Fourier transform," *Appl. Comput. Harmon. Anal.*, vol. 16, no. 3, pp. 182–202, May 2004.

[8] K. Sun, M. Elhajj, and W. Y. Ochieng, "A GNSS anti-interference method based on fractional Fourier transform," *IEEE Trans. Aerosp. Electron. Syst.*, vol. 60, no. 5, pp. 5636–5650, Oct. 2024.

[9] K. Sun, B. Yu, L. Xu, M. Elhajj, and W. Yotto Ochieng, "A novel GNSS anti-interference method using fractional Fourier transform and notch filtering," *IEEE Trans. Instrum. Meas.*, vol. 73, 2024, Art. no. 8507617.

[10] X. Álvarez Molina, G. Seco-Granados, and J. A. López-Salcedo, "Chirp interference mitigation in snapshot GNSS receivers using the time-frequency ridge-assisted fractional Fourier transform," in *Proc. Int. Conf. Localization GNSS*, 2025, pp. 1–7.

[11] J. Song, Y. Wang, and Y. Liu, "Iterative interpolation for parameter estimation of LFM signal based on fractional Fourier transform," *Circuits, Syst., Signal Process.*, vol. 32, no. 3, pp. 1489–1499, 2013.

[12] S. Meignen, T. Gardner, and T. Oberlin, "Time-frequency ridge analysis based on the reassignment vector," in *Proc. Eur. Signal Process. Conf.*, 2015, pp. 1486–1490.

[13] D. Iatsenko, P. V. McClintock, and A. Stefanovska, "Extraction of instantaneous frequencies from ridges in time–frequency representations of signals," *Signal Process.*, vol. 125, pp. 290–303, 2016.

[14] Matlab Mathworks R2024b, "Time-frequency ridges," (n.d.). [Online]. Available: https://uk.mathworks.com/help/signal/ref/tfridge.html

[15] G. H. Golub, M. Heath, and G. Wahba, "Generalized cross-validation as a method for choosing a good ridge parameter," *Technometrics*, vol. 21, no. 2, pp. 215–223, 1979.
[16] L. M. Chaves, L. D. D. Carvalho, C. J. D. Reis, and D. J. D. Souza, "Explaining the generalized cross-validation on linear models," *J. Math. Statist.*, vol. 15, no. 1, pp. 298–307, 2019.
[17] A. V. Oppenheim and R. W. Schafer, Eds., *Discrete-time Signal Processing (Prentice Hall Signal Processing Series)*, 3rd ed. Upper Saddle River, NJ, USA: Pearson, 2010.
[18] D. Borio and P. Closas, "Complex signum non-linearity for robust GNSS interference mitigation," *IET Radar, Sonar Navigation*, vol. 12, no. 8, pp. 900–909, 2018.
[19] Å. Björck, *Numer. Methods for Least Squares Problems*, Philadelphia, PA, USA: SIAM, 1996.
[20] D. Jiménez-Baños, N. Blanco-Delgado, G. López-Risueño, G. Seco-Granados, and A. Garcia-Rodriguez, "Innovative techniques for GPS indoor positioning using a snapshot receiver," in *Proc. Int. Tech. Meeting Satell. Division Inst. Navigation*, 2006, pp. 2944–2955.
[21] G. Seco-Granados, J. López-Salcedo, D. Jiménez-Baños, and G. López-Risueño, "Challenges in indoor global navigation satellite systems: Unveiling its core features in signal processing," *IEEE Signal Process. Mag.*, vol. 29, no. 2, pp. 108–131, Mar. 2012.
[22] T. Pany et al., "GNSS software-defined radio: History, current developments, and standardization efforts," *NAVIGATION: J. Inst. Navigation*, vol. 71, no. 1, 2024, Art. no. navi.628.

Xavier Álvarez-Molina (Graduate Student Member, IEEE) was born in Martorell, Spain. He received the double degree in Telecommunication Systems Engineering Computer Science (Information Technology Specialization) in 2024 from the Universitat Autònoma de Barcelona, Bellaterra, Spain, where he is currently working toward the master's degree in telecommunications engineering.

He is currently a Technical Research Assistant with the SPCOMNAV research group, Universitat Autònoma de Barcelona. His research interests include GNSS signal processing, time–frequency analysis, and interference suppression.

Gonzalo Seco-Granados (Fellow, IEEE) received the Ph.D. degree in telecommunications engineering from the Universitat Politècnica de Catalunya, Barcelona, Spain, in 2000, and the M.B.A. degree in business administration from IESE Business School, Barcelona, in 2002.

From 2002 to 2005, he was a Member of the European Space Agency, Noordwijk, The Netherlands, where he contributed to the design of the Galileo system. He is currently a Professor with the Department of Telecommunications, Universitat Autònoma de Barcelona, Barcelona, where he was the Coordinator of the Telecommunications Engineering Degree from 2007 to 2010 and the Vice Dean of the Engineering School from 2011 to 2019. He is also with the Institute of Space Studies of Catalonia, Barcelona. In 2015, 2019, and 2022, he was a Fulbright Visiting Scholar with the University of California, Irvine, CA, USA. He is the Co-Founder of Loctio, a start-up offering low-energy Global Navigation Satellite System positioning solutions for Internet of Things. His research interests include signal processing and signal/receiver design for GNSS, low Earth orbit positioning, navigation, and timing, beyond 5G-integrated communications, localization, and sensing.

Dr. Seco-Granados was the recipient of the 2021 IEEE Signal Processing Society's Best Paper Award. He was a Member of IEEE Signal Processing Society Sensor Array and Multichannel Technical Committee from 2019 to 2024. He is an ICREA Academia Fellow. Since 2022, he has been a Member of the EURASIP Signal Processing for Multisensor Systems Technical Committee. From 2018 to 2025, he was the President of the Spanish Chapter of the IEEE Aerospace and Electronic Systems Society.

José A. López-Salcedo (Senior Member, IEEE) received the M.Sc. and Ph.D. degrees in telecommunication engineering from the Universitat Politècnica de Catalunya, Barcelona, Spain, in 2001 and 2007, respectively.

Since 2006, he has been with the Universitat Autònoma de Barcelona, Barcelona, where he is currently a Professor, and was the Coordinator of the Telecommunications Engineering degree from 2011 to 2019. He is also with the Institute of Spatial Studies of Catalonia and Co-Founder of the start-up company Loctio. He has held several visiting appointments with the University of Illinois at Urbana–Champaign, Urbana, IL, USA; the University of California at Irvine, Irvine, CA, USA; the European Commission Joint Research Center. He is the Principal Investigator of more than 25 research projects, most of them funded by the European Space Agency on topics dealing with signal processing for GNSS receivers. His research interests include signal processing for communications and navigation, and the convergence among GNSS, 5G/6G, and LEO satellites for positioning, navigation, and timing.

Dr. López-Salcedo is the Chair of the IEEE Aerospace and Electronic Systems Society (AESS) Spain Chapter, a Member of the Editorial Committee of the Korean Institute of Positioning, Navigation, and Timing, and an Elected Member of the IEEE Signal Processing Society Sensor Array and Multichannel Technical Committee.